ORIGINAL ARTICLE

MeCP2 co-ordinates liver lipid metabolism with the NCoR1/HDAC3 corepressor complex

Stephanie M. Kyle[1,2], Pradip K. Saha[3], Hannah M. Brown[2,†], Lawrence C. Chan[3] and Monica J. Justice[1,2,4,*]

[1]Genetics and Genome Biology Program, The Hospital for Sick Children, The Peter Gilgan Centre for Research and Learning, Toronto, ON M5G 0A4, Canada, [2]Department of Molecular and Human Genetics, [3]Department of Medicine, Division of Diabetes, Endocrinology and Metabolism, Baylor College of Medicine, Houston, TX 77030, USA and [4]Department of Molecular Genetics, University of Toronto, Toronto, ON M5S 1A1, Canada

*To whom correspondence should be addressed at: Tel: +416-813-7654; Fax: 416-813-4931; Email: monica.justice@sickkids.ca

Abstract

Rett syndrome (RTT; OMIM 312750), a progressive neurological disorder, is caused by mutations in methyl-CpG-binding protein 2 (*MECP2*; OMIM 300005), a ubiquitously expressed factor. A genetic suppressor screen designed to identify therapeutic targets surprisingly revealed that downregulation of the cholesterol biosynthesis pathway improves neurological phenotypes in *Mecp2* mutant mice. Here, we show that MeCP2 plays a direct role in regulating lipid metabolism. *Mecp2* deletion in mice results in a host of severe metabolic defects caused by lipid accumulation, including insulin resistance, fatty liver, perturbed energy utilization, and adipose inflammation by macrophage infiltration. We show that MeCP2 regulates lipid homeostasis by anchoring the repressor complex containing NCoR1 and HDAC3 to its lipogenesis targets in hepatocytes. Consistently, we find that liver targeted deletion of *Mecp2* causes fatty liver disease and dyslipidemia similar to HDAC3 liver-specific deletion. These findings position MeCP2 as a novel component in metabolic homeostasis. Rett syndrome patients also show signs of peripheral dyslipidemia; thus, together these data suggest that RTT should be classified as a neurological disorder with systemic metabolic components. We previously showed that treatment of *Mecp2* mice with statin drugs alleviated motor symptoms and improved health and longevity. Lipid metabolism is a highly treatable target; therefore, our results shed light on new metabolic pathways for treatment of Rett syndrome.

Introduction

Mutations in the X-linked gene encoding methyl-CpG-binding protein 2 (*MECP2*) are the primary cause of the neurological condition Rett syndrome (1). Females with loss-of-function mutations in *MECP2* achieve developmental milestones during the first 6–18 months of life, followed by progressive loss of acquired linguistic and motor skills, stereotypic hand movements, difficulty walking, irregular breathing, and seizures. *MECP2* hemizygous males typically die perinatally of encephalopathy. However, *Mecp2* hemizygous (*Mecp2*/Y) male mice survive through birth and develop Rett syndrome (RTT)-like symptoms beginning at 4 weeks of age that progressively worsen until death occurs between 6 and 12 weeks. *Mecp2*/Y mice are the primary model of RTT; their study has been vital towards understanding the etiology of the disease as *Mecp2* heterozygous

(*Mecp2*/+) female mice have a wide range in phenotype severity due to random X-chromosome inactivation (2–5).

Mecp2 encodes a ubiquitously-expressed, intrinsically disordered protein (IDP) that, in murine neurons, binds DNA at near histone-octomer levels (6,7). Characteristic of an IDP, MeCP2 is targeted by a multitude of post-translational modifications, which determine cofactor association and may account for its seemingly endless roles in maintaining cellular homeostasis (8). To this effect, the mechanistic contribution of mutant MeCP2 to RTT pathology is highly complex and remains elusive.

As the culprit gene of a devastating neurological disorder, *MECP2* has been largely studied in relation to central nervous system (CNS) development, maturation, and signaling. In neurons, MeCP2 can repress gene transcription by binding the nuclear receptor co-repressor/silencing mediator for retinoid or thyroid-hormone receptors (NCoR/SMRT) complex at MeCP2 amino acids 302–306 (9,10). MeCP2-NCoR/SMRT suppresses transcription by delivering the histone deacetylase HDAC3 to target genes, which removes acetyl marks left by histone acetyltransferases, resulting in a closed chromatin state (11,12). A R306C missense mutation in mouse *Mecp2* abolishes interaction with the NCoR/SMRT co-repressor complex and prevents MeCP2-mediated transcriptional repression. Importantly, this mutation is sufficient to cause severe RTT-like phenotypes, including hindlimb clasping, hypoactivity, and reduced brain weight, thus highlighting the importance of the NCoR/SMRT-HDAC3 interaction with MeCP2 in RTT pathology. Furthermore, the amino acid 302–306 region of human *MECP2* contains a missense mutation hotspot, causing classical RTT in patients (10,13).

Mouse models have established the vital role of the NCoR co-repressor complex in energy metabolism. NCoR-HDAC3 regulates the circadian metabolic cycle of the liver, governing the fluctuation between lipid and glucose utilization in hepatocytes during light/dark cycles (14,15). Loss of *Hdac3* from the liver of embryonic or adult mice promotes a constitutively active transcriptional environment, which increases expression of *de novo* lipogenesis enzymes, resulting in fatty liver disease (16,17). Further, *Hdac3* liver deletion increases transcription of several genes in the cholesterol biosynthesis pathway, elevating serum cholesterol. One target of HDAC3 is squalene epoxidase (*Sqle*), a rate-limiting enzyme of the committed cholesterol biosynthesis pathway, whose transcription is increased ∼170-fold in response to *Hdac3* liver deletion (16,18,19). Curiously, a forward genetic suppressor screen found that a nonsense mutation in *Sqle* improved RTT-like motor symptoms and overall health in *Mecp2* null mice. This was intriguing, as both RTT patients and *Mecp2* mutant mice can have increased serum cholesterol and triglycerides (20–22). Furthermore, treatment of *Mecp2* hemizygous male and heterozygous female mice with HMG-CoA reductase inhibitors (statins) phenocopies symptom improvement by *Sqle* mutation (20). Notably, RTT-like phenotypes are improved following treatment with fluvastatin, a hydrophilic statin that does not readily cross the blood-brain barrier suggesting that MeCP2 plays a role in regulating systemic cholesterol metabolism (23,24). As such, we hypothesized that genetic loss of *Mecp2* would cause metabolic perturbations in mice. Here, we report that *Mecp2* deletion causes fatty liver disease, metabolic syndrome, insulin resistance, and alters overall energy homeostasis. We show that hepatic MeCP2 works in conjunction with the NCoR-HDAC3 corepressor complex to orchestrate transcription of enzymes in the triglyceride and cholesterol synthesis pathways. In support of this, liver-specific loss of *Mecp2* is sufficiently deleterious to increase lipogenic enzyme transcription leading to fatty liver; however, these mice are insulin sensitive, suggesting that MeCP2 plays a role in insulin signaling outside of the liver.

Results

Mecp2 deletion increases lipogenic enzyme expression, resulting in non-alcoholic fatty liver

Surprisingly, we observed a consistent pale coloration of 129.*Mecp2*/Y livers (Fig. 1A). Oil Red O staining suggested an accumulation of lipid vesicles and subsequent quantification of lipids in *Mecp2*/Y null liver showed a ∼2-fold increase in liver triacylglycerol (TAG) over wild-type (Fig. 1B). We examined hepatic expression of genes in the fatty acid and TAG synthesis pathways at three (pre-symptomatic) and eight (symptomatic) weeks of age. Expression of four enzymes involved in fatty acid synthesis (acetyl-CoA carboxylase A and B [*Acca*, *Accb*], fatty acid synthase [*Fasn*] and stearoyl-CoA desaturase 1 [*Scd-1*]) was increased in pre- and post-symptomatic *Mecp2*/Y mice liver. Expression of fatty acid translocase (*Cd36*), a transporter of fatty acids, and perilipin 2 and 5 (*Plin2* and *Plin5*), proteins that coat TAG-dense lipid droplets, was also increased. However, levels of sterol-regulatory element-binding protein 1c (*Srebp-1c*), the transcription factor responsible for regulating the fatty acid synthesis pathway, was not altered in *Mecp2*/Y liver (Fig. 1C–E) (25,26).

Transcription of HMG-CoA reductase (*Hmgcr*), squalene epoxidase (*Sqle*) and lanosterol synthase (*Lss*), enzymes of the cholesterol biosynthesis pathway, were all increased ∼3-fold in 129.*Mecp2*/Y liver by 8 weeks of age (Fig. 1C–E). Concurrently, 129.*Mecp2*/Y null mice have increased serum cholesterol by six weeks of age (20). Therefore, we analyzed the expression and maturation of SREBP2, the transcription factor responsible for expression of enzymes in the cholesterol biosynthesis pathway (27). However, there were no differences in levels of *Srebp2* transcript (Fig. 1C and D) nor levels of unspliced or mature nuclear nSREBP2 between 129.*Mecp2*/Y null and wild-type livers (Fig. 1F and G). These data suggest that a SREBP-independent pathway is responsible for aberrant hepatic lipogenesis in *Mecp2*/Y null mice. Notably, *Mecp2*/+ heterozygous female mice also accumulate fat in their livers by 6 months of age, indicating that mosaic loss of *Mecp2* is sufficient to cause fatty liver (Supplementary Material, Figure S1A and B).

Impaired glucose and insulin homeostasis in *Mecp2* mice

Non-alcoholic fatty liver disease is closely linked to glucose intolerance and insulin resistance. *Mecp2*/Y mice display hyperglycemia in the fed state at 8-weeks of age, but glucose levels are similar to wild-type when fasted (Supplementary Material, Figure S2A and B). Even so, plasma insulin levels of fasted and nonfasted *Mecp2*/Y mice are significantly greater than wild-type littermates at both pre- and post-symptomatic ages (4 and 8 weeks, respectively) (Fig. 2A and B). Concurrently, 129.*Mecp2*/Y null mice are glucose intolerant at both four and eight-weeks of age and insulin resistance is apparent by 9-weeks (Supplementary Material, Figure S2C–E). Glucose intolerance also arises in 129.*Mecp2*/+ heterozygous females by 20-weeks of age and insulin resistance is evident at 24-weeks of age (Supplementary Material, Figure S3A–C).

To critically assess global insulin sensitivity, *Mecp2*/Y null mice were subjected to hyperinsulinemic-euglycemic clamp studies (Fig. 2C). In this gold standard assay for assessing insulin resistance, [3-³H]-glucose and insulin are infused in fasted, unrestrained mice to maintain a euglycemic 'clamped' state
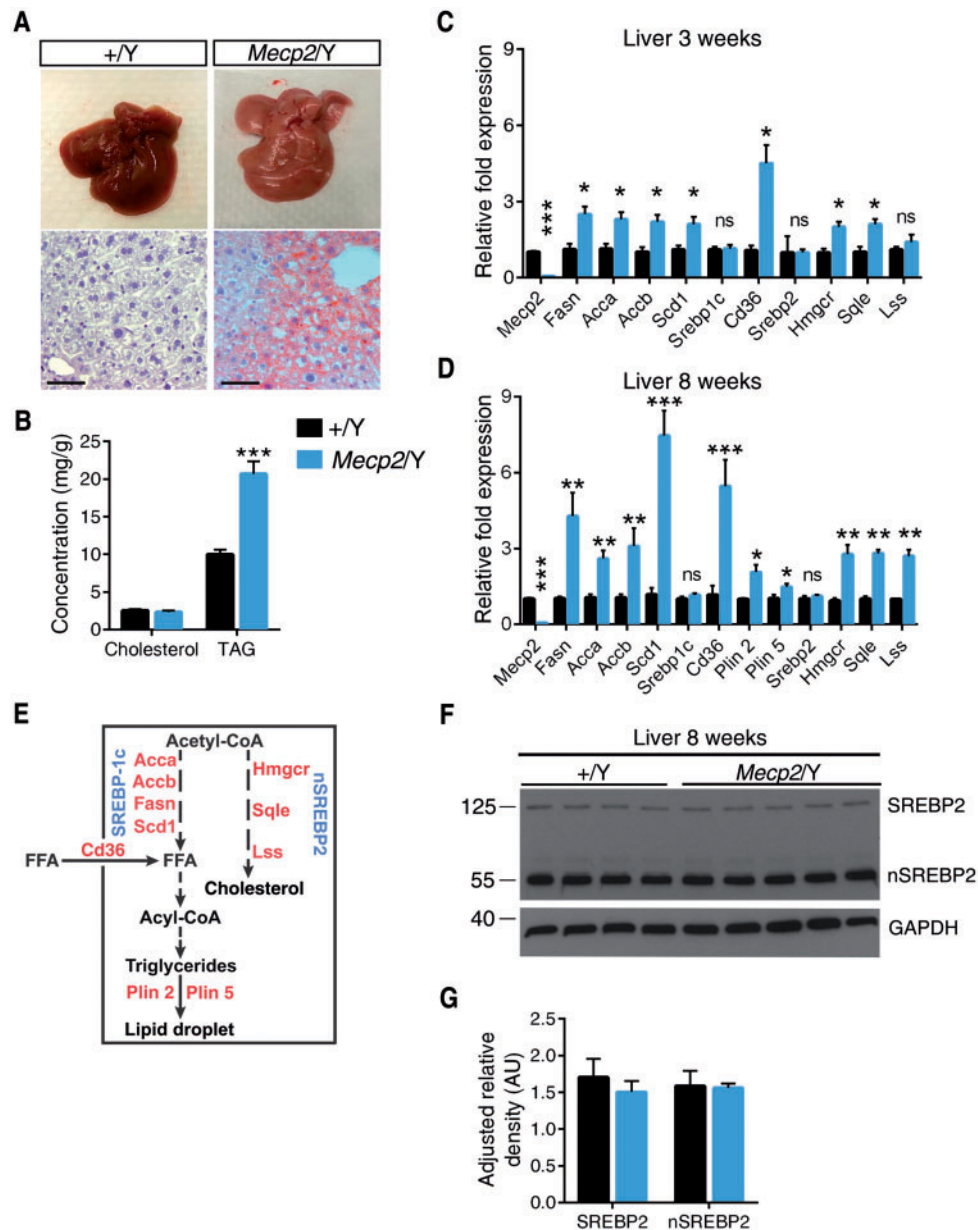
Figure 1. *Mecp2* null mice develop fatty liver and aberrant hepatic lipogenic enzyme expression. **(A)** Representative livers from eight-week old mice. Liver sections were subjected to Oil Red O staining. Scale bar represents 50 μM. **(B)** Levels of TAGs and total cholesterol in liver of eight-week old male mice (n = 6–7 mice per genotype). **(C)** mRNA expression in liver dissected from three-week old male mice (n = 3–4 mice per genotype) quantified by real-time PCR. **(D)** mRNA expression in liver dissected from eight-week old male mice (n = 6–7 mice per genotype) quantified by real-time PCR. **(E)** A simplified schematic of the enzymes and transcription factors in the hepatic cholesterol and TAG synthesis pathways. **(F)** Western blot of immature SREBP2 and mature, nuclear SREBP2 (nSREBP2) in liver lysates from eight-week old male *Mecp2/Y* mice (n = 4–5 mice per genotype). **(G)** Quantification of nSREBP2/SREBP2 western blot normalized to GAPDH. B–D, G. Values are mean $\pm$ SEM. ns, no significance; *$P < 0.05$, **$P \leq 0.01$, ***$P < 0.001$ versus wild-type littermates. Statistical analyses were performed using Student's t-test.

(100–140 mg/dl serum glucose). The radioisotope allows for measurement of basal and clamped hepatic glucose production (HGP) and glucose disappearance or disposal (Rd). These studies revealed that *Mecp2/Y* null mice require a lower rate of exogenous glucose infusion (GIR) to maintain euglycemia (Fig. 2D). When clamped, insulin infusion did not decrease HGP in mutant mice (Fig. 2E). Further, *Mecp2/Y* mice have a lower rate of whole-body insulin-stimulated glucose disposal (Rd) (Fig. 2F). Together, these data reflect a state of profound insulin resistance in *Mecp2* null liver, skeletal muscle, and white adipose tissues (WATs). To this effect, glucose uptake by *Mecp2* null WAT and muscle is markedly suppressed (Fig. 2G). However, glucose uptake is increased in the

cerebral cortex and hypothalamus/thalamus regions of the brain, possibly due to the insulin-independent nature of the major glucose transporters (GLUTs) of the brain.

Mecp2 deletion induces macrophage infiltration, adipose inflammation and increased lipolysis

Lipolysis is precisely regulated by hormones such as insulin. We asked whether *Mecp2* loss and subsequent insulin resistance would affect adipose lipolysis. Basal levels of circulating glycerol and non-esterified fatty acids (NEFA) were significantly
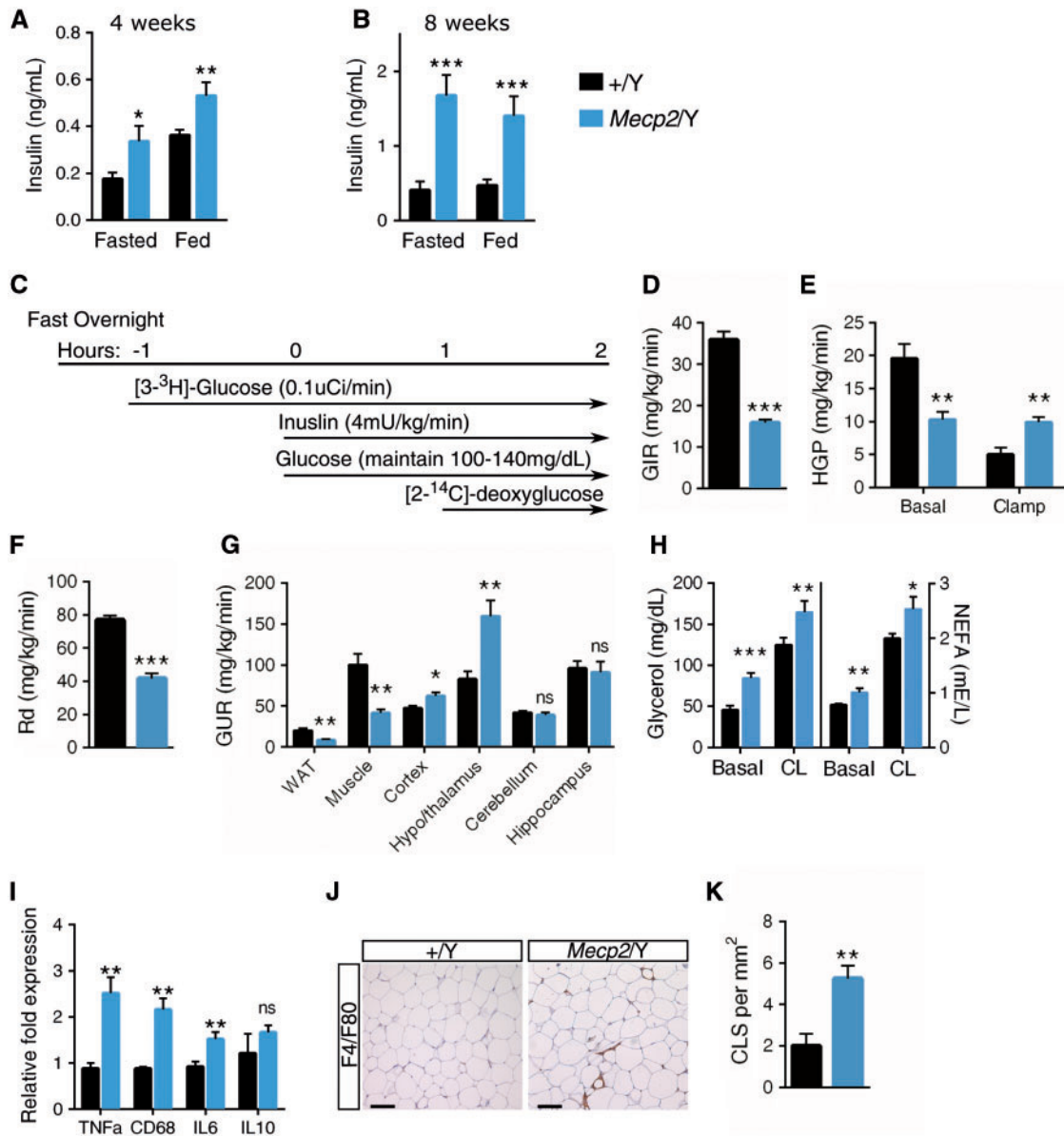
Figure 2. *Mecp2* null mice are insulin resistant, resulting in perturbed glucose uptake. **(A)** Serum insulin concentration in *Mecp2*/Y and wild-type (+/Y) littermates at four-weeks of age in the fed state (*n* = 5–7 mice per genotype) or following a 6-h fast (*n* = 10–12 mice per genotype). **(B)** Serum insulin concentration at eight-weeks of age in the fed state or following a 6-h fast (*n* = 10–12 mice per genotype). **(C)** A schematic showing the hyperinsulinemic-euglycemia clamps protocol (*n* = 4–5 mice per genotype) performed at eight-weeks of age. **(D)** The GIR needed to maintain euglycemia (100–140 mg/dl serum glucose) in response to insulin clamps. **(E)** HGP in the basal and clamped state. **(F)** Rate of insulin-stimulated glucose disposal (Rd). **(G)** The rate of glucose uptake in WAT, muscle, cerebral cortex, hypothalamus and thalamus, cerebellum, and hippocampus. **(H)** *In vivo* lipolysis assays in 4-h fasted male mice at eight-weeks of age. Serum glycerol and NEFAs levels are shown at basal metabolic state (basal) and 15-min after lipolysis induction by injection with CL316243 (CL), a β_3-adrenoceptor agonist (*n* = 7–9 mice per genotype). **(I)** mRNA expression of inflammatory markers TNFa, CD68, IL6, and IL10 in epididmal WAT from eight-week male mice (*n* = 6–8 mice per genotype) quantified by real-time PCR. **(J)** Representative epididymal WAT sections stained for F4/F80+ cells at eight-weeks. Scale bar represents 100 μM. **(K)** Number of crown-like structures in epididymal WAT sections (*n* = 3 mice per genotype) at 9-weeks. A,B, D–I, K. Values are mean ± SEM. ns, no significance, *$P < 0.05$, **$P \leq 0.01$, ***$P \leq 0.001$ versus wild-type littermates. Statistical analyses were performed using Student's *t*-test.

increased at eight-weeks in *Mecp2*/Y null mice and at 24-weeks in *Mecp2*/+ heterozygous female mice compared with wild-type littermates (Fig. 2H and Supplementary Material, Figure S3D), suggesting an increased rate of lipolysis. A selective β_3-adrenergic receptor agonist CL316243 (CL), was used to measure response to lipolysis induction. Lipolysis stimulation resulted in an approximately 2-fold increase in circulating glycerol and fatty acids in both male and female *Mecp2* mutant and wild-type mice (Fig. 2H and Supplementary Material, Figure S3D).

No increase in basal circulating NEFA or glycerol was observed when lipolysis was examined at earlier time points (4-weeks of age in *Mecp2*/Y males and 12-weeks of age in *Mecp2*/+ females), indicating that glucose intolerance precedes these events (Supplementary Material, Figures S2F and S3E).

Adipose expansion and increased lipolysis are often accompanied by WAT inflammation. As such, we investigated inflammatory markers in serum and in epididymal (gonadal) WAT using gene expression analysis. Serum leptin, a pro-inflammatory
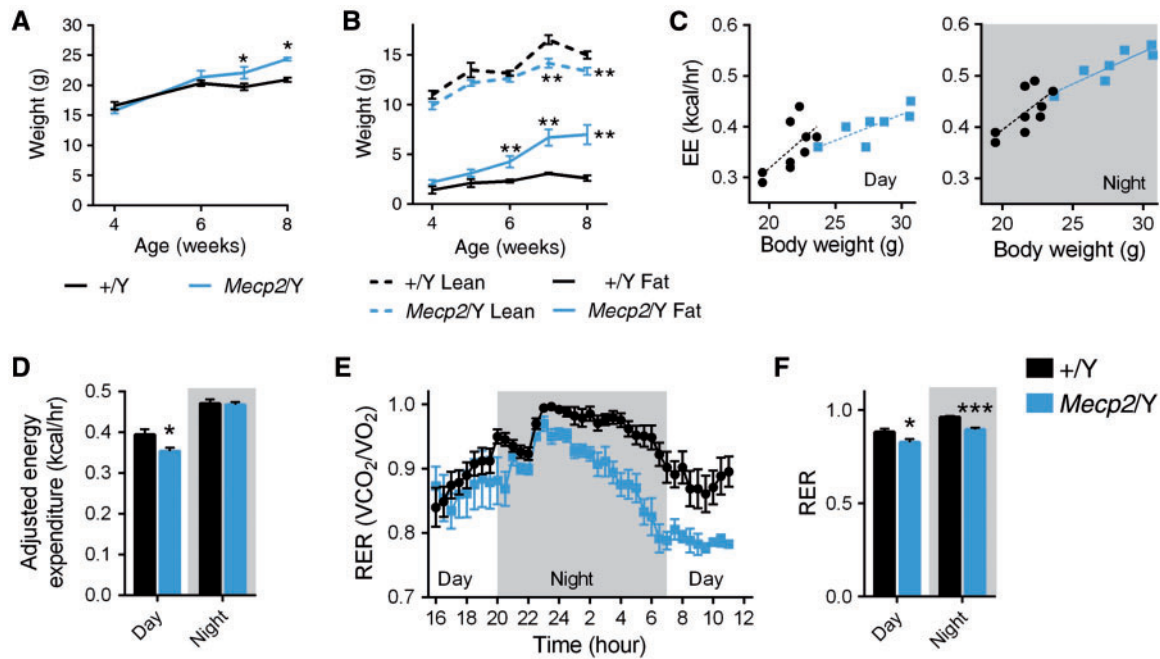
Figure 3. *Mecp2* deletion shifts whole body substrate metabolism. **(A)** Total weight of *Mecp2*/Y and wild-type (+/Y) littermates ($n = 10$ mice per genotype). **(B)** Lean and fat mass ($n = 7$–8 mice per genotype). **(C)** Linear regression for EE as a function of genotype and body weight, separated by day (+/Y: $y = 0.0228 * x - 0.1398$; $r^2 = 0.4247$; *Mecp2*/Y: $y = 0.0102 * x + 0.1159$; $r^2 = 0.6417$) and night (+/Y: $y = 0.0209 * x - 0.0245$; $r^2 = 0.4716$; *Mecp2*/Y: $y = 0.0125 * x + 0.1709$; $r^2 = 0.7990$) periods. **(D)** EE adjusted for weight (average weight = 24.35g) using ANCOVA for wild-type control and *Mecp2*/Y mice ($n = 7$–9 mice per genotype) at eight-weeks. **(E)** Respiratory rate (VCO_2/VO_2) across a 20-h period. **(F)** Average respiratory rate, separated by day and night periods. Values are mean ± SEM. ns, no significance, *$P < 0.05$, ** $P \leq 0.01$, *** $P \leq 0.001$ versus WT. EE averages were adjusted for weight using ANCOVA and statistical analyses were performed using Student's *t*-test.

factor, was highly elevated in *Mecp2*/Y serum while there was no observable difference in adiponectin (Supplementary Materials, Figure S2G and H). *Mecp2*/Y null WAT has increased expression of macrophage-derived interleukin-6 (IL-6) and TNFα, cytokines implicated in dramatically increasing adipocyte lipolysis, and CD68, a macrophage marker, but exhibit no change in the anti-inflammatory marker IL10 (28) (Fig. 2I). These data indicate macrophage infiltration in *Mecp2*/Y WAT, which was confirmed by increased F4/F80 immunohistochemistcal staining in gonadal WAT (Fig. 2J). Adipose macrophages in *Mecp2*/Y null WAT formed a significantly larger number of crown-like structures, which envelope necrotic adipocytes (Fig 2K).

Mecp2 deletion modifies whole body substrate metabolism

To further characterize metabolic changes in *Mecp2*/Y null mice, we assessed energy expenditure (EE) and substrate metabolism by indirect calorimetry over a 20-h period (11-h dark period, cumulative 9-h day period), following a 4-h acclimation period. 129.*Mecp2*/Y null male mice weigh significantly more than wild-type (+/Y) littermates by seven weeks of age, due to an expansion of white and brown adipose tissue, despite a decrease in lean mass (Fig. 3A and B and Supplementary Material, Figure S4A and B). Because *Mecp2*/Y mice are heavier at eight weeks of age, we employed analysis of covariance (ANCOVA) to control for both the weight factor and genotype (29) (Fig. 3C). *Mecp2*/Y null mice display a slight, but significant decrease ($P = 0.03$) in EE during the day, but have no difference in EE at night (Fig. 3D). This is somewhat surprising considering severe hypoactivity is a hallmark of symptomatic (eight-week old) *Mecp2*/Y null mice

(3). As expected, both wild-type and *Mecp2* null mice displayed diurnal rhythms in their whole-body EE and respiratory exchange ratio (RER). RER, an indicator of energy derived from oxidizing glucose (RER = 1.0) or fatty acids (RER = 0.7), increases for both genotypes at night, reflective of food intake and carbohydrate utilization (Fig. 3E). However, *Mecp2* null mice have a markedly decreased RER versus wild-type littermates during both day and night cycles, consistent with preferential lipid oxidation over carbohydrate metabolism (Fig. 3E and F).

MeCP2 regulates expression of liver lipogenic enzymes through interaction with the NCoR/HDAC3 corepressor complex

In neurons, MeCP2 interacts with the nuclear receptor corepressor 1 (NCoR1) complex, which includes the proteins histone deacetylase 3 (HDAC3) and transducin-(beta) like 1 X-linked receptor 1 (TBLR1) to facilitate gene repression (9,10). In hepatocytes, the NCoR-HDAC3-TBLR1 corepressor complex is a potent regulator of deactylase-dependent gene transcription. As such, we hypothesized that this corepressor complex contributes to the metabolic perturbations in *Mecp2* null mice. To address this question, we first assessed native MeCP2 ability to bind the NCoR complex *in vivo*, in the liver. Co-immunoprecipitation of HDAC3 indeed revealed association with MeCP2, as well as its corepressor complex partners NCoR1 and TBLR1 (Fig. 4A). This binding partnership was validated using three different HDAC3 immunoprecipitation (IP) antibodies, all of which pulled down MeCP2 in complex (not shown).

Next, we investigated the effect of MeCP2 loss on HDAC3 binding and activity. Specifically, we performed ChIP-qPCR to
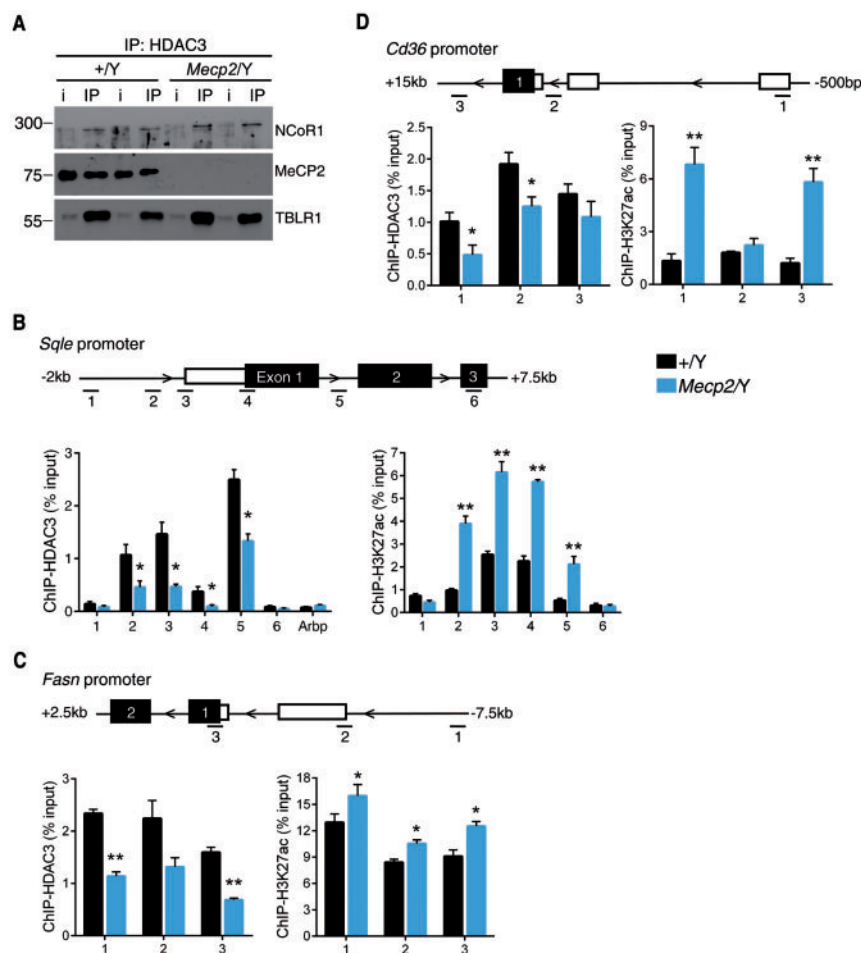
Figure 4. MeCP2 interacts in murine hepatocytes with the NCoR-HDAC3 complex and loss of MeCP2 prevents lipogenic enzyme repression at the locus. **(A)** IP of NCoR1, MeCP2, and TBLR1 from murine liver nuclear extracts using an antibody to HDAC3. i, input. **(B)** Anti-HDAC3 and anti-H3K27ac ChIP-qPCR of sites surrounding the *Sqle* TSS (*n* = 3 mice per genotype). **(C)** Anti-HDAC3 and anti-H3K27ac ChIP-qPCR of sites surrounding the *Fasn* TSS (*n* = 3 mice per genotype). **(D)** Anti-HDAC3 and anti-H3K27ac ChIP-qPCR of sites surrounding the *Cd36* TSS (*n* = 3 mice per genotype). Values are mean ± SEM. ns, no significance, *P < 0.05, ** P ≤ 0.01, *** P ≤ 0.001 versus WT. Statistical analyses were performed using Student's *t*-test.

assess the binding of HDAC3 to regulatory regions surrounding the transcription start sites (TSS) of several rate-limiting enzymes that are upregulated in *Mecp2* null liver. We found that loss of MeCP2 significantly hinders the capability of HDAC3 to bind regulatory regions surrounding the TSS of *Sqle* (Fig. 4B), *Fasn* (Fig. 4C), and *Cd36* (Fig. 4D) in the liver. HDAC3 binding at the promoter region of the attachment region binding protein (*Arbp*) gene was used as a negative control (Fig. 4B). Deletion of HDAC3 from the liver or genetic abolishment of its deacetylase activity results in increased local histone acetylation in liver, specifically of the transcriptional activating marker Histone 3 lysine 27 acetylation (H3K27ac) (15,16,30). Therefore, we hypothesized that a reduction in chromatin-bound HDAC3 in *Mecp2* null mice would result in increased H3K27ac at the same locations. Remarkably, we saw increased accumulation of H3K27ac at all three genes in *Mecp2* null liver lysates, correlating with decreased HDAC3 binding (Fig. 4B–D).

A conditional deletion of *Mecp2* from mouse liver dissociates fatty liver and insulin resistance

In light of these findings, we hypothesized that *Mecp2* loss from the liver alone would be sufficient to cause fatty liver disease

through aberrant expression of genes such as *Sqle*. To test this hypothesis, we generated a B6.*Mecp2* liver-specific deleted mouse line. We removed *Mecp2* from *Albumin*-expressing cells by breeding B6.*Mecp2*^tm1Bird^ mice (*Mecp2*^flox/+^), in which exons 3 and 4 are flanked by *loxP* sites, to B6.*Alb*-Cre^21Mgn^ BAC transgenic mice. *Alb* regulatory elements drive Cre expression in transgenic mice during embryonic development (as early as E15.5) and after birth in hepatocytes, with some restricted expression in bile ducts. Recombination of the floxed *Mecp2* allele is robust but not complete in the *Mecp2*^flox^/Y;*Alb*-Cre liver, resulting in a ~90% decrease in *Mecp2* transcription, as evidenced by qRT-PCR (Fig. 5A). However, recombination does not occur in the brain of *Mecp2*^flox^/Y;*Alb*-Cre mice and they did not develop neurological symptoms, as expected (Supplementary Material, Figure S5A and B). It is important to note that the *Mecp2*^flox^ allele (*Mecp2*^tm1Bird^) utilized in these studies is hypomorphic, resulting in an approximate 20% decrease in *Mecp2* mRNA in littermate control males lacking Cre (Fig. 5B) (31). Therefore, we anticipated that male mice carrying this allele would display mild phenotypes due to a decrease in MeCP2 dosage.

Conditional deletion of *Mecp2* from hepatocytes increases transcription of genes in the lipogenesis pathways, including the rate-limiting enzymes of cholesterol biosynthesis *Hmgcr* and *Sqle*,
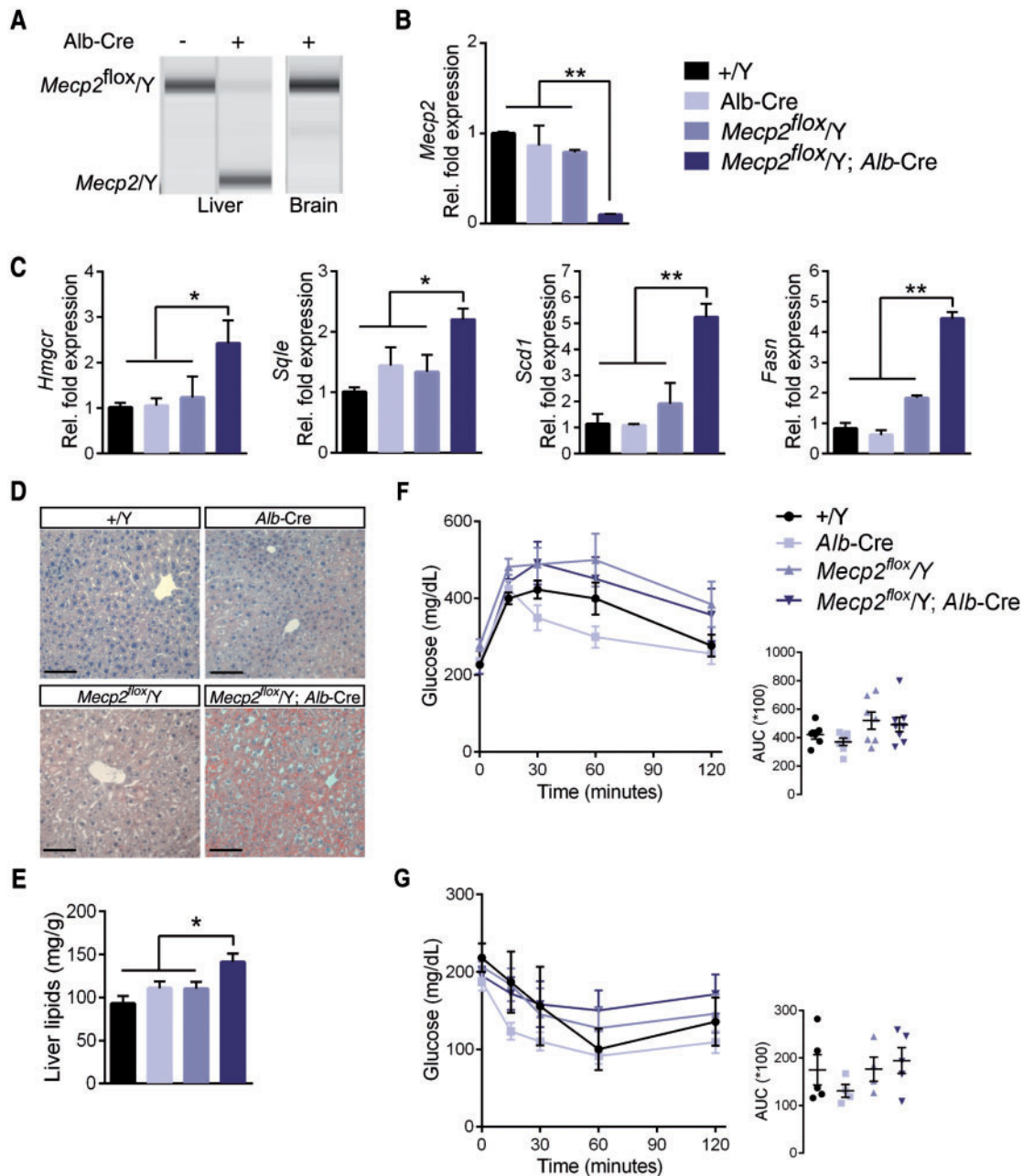
Figure 5. Loss of *Mecp2* from the liver dissociates fatty liver and insulin resistance. **(A)** PCR amplification of the *Mecp2* locus in mouse liver shows presence of a hemizygous *Mecp2flox* allele in mice lacking the *Alb*-Cre transgene. Offspring with the genotype *Mecp2flox*/Y; *Alb*-Cre have recombination of the *Mecp2* floxed locus to a null allele. This recombination does not occur in the brain of *Mecp2flox*/Y; *Alb*-Cre mice. **(B)** *Mecp2* mRNA expression in liver ($n = 5$ per genotype). **(C)** mRNA expression in liver dissected from 6-month old male mice ($n = 5$ per genotype). **(D)** Livers from 6-month-old mice subjected to Oil Red O staining. Scale bar represents 100 μM. **(E)** Levels of liver lipids of from 6-month-old male mice (n = 6–7 per genotype). **(F)** Glucose tolerance tests (GTT). Glucose was administered intraperitoneally after a 5-h fast, and blood glucose was measured at the indicated times. Male mice were tested at 6 months of age ($n = 6$–8 mice per genotype). **(G)** Insulin tolerance tests (ITT). Insulin was administered intraperitoneally after a 4-h fast, and blood glucose was measured at the indicated times. Male mice were tested at 6 months of age ($n = 4$–5 mice per genotype). B–C, E–G. Values are mean ± SEM. ns, no significance, * $P < 0.05$, ** $P \leq 0.01$, *** $P \leq 0.001$. Statistical analyses were performed using one-way analysis of variance (ANOVA) followed by Tukey's *post-hoc* analysis.

as well as rate-limiting enzymes of the triglyceride synthesis pathway *Scd1* and *Fasn* (Fig. 5C). Similarly to a liver-specific deletion of *Hdac3*, B6.*Mecp2flox*/Y;*Alb*-Cre mice develop fatty liver, as evidenced by Oil Red O staining and a quantitative assessment of liver lipids (Fig. 5D and E). Perturbation of these pathways translates to an increase in serum cholesterol in B6.*Mecp2flox*/Y;*Alb*-Cre, but not in wild-type, *Alb*-Cre, or B6.*Mecp2flox*/Y littermate controls (Table 1). B6.*Mecp2flox*/Y;*Alb*-Cre mice gain weight through an

expansion of fat mass; however, B6.*Mecp2flox*/Y littermates display the same phenotype. Therefore, we cannot attribute weight gain to a direct MeCP2 mechanism in the liver.

Fatty liver is closely associated with metabolic syndrome; therefore, we performed glucose tolerance and insulin resistance tests in tissue-specific deleted B6.*Mecp2* null animals and control littermates. *Mecp2flox*/Y;*Alb*-Cre mice are not glucose intolerant nor insulin resistant (Fig. 5F and G). Furthermore,

Table 1. Metabolic and serum parameters in liver-specific *Mecp2* null mice

Parameter	6 months			
	B6.+/Y	B6.Alb-Cre	B6.Mecp2^{flox}/Y	B6.Mecp2^{flox}/Y; Alb-Cre
Weight (g)	33.8 ± 0.8	35.6 ± 0.8[ns]	41.7 ± 1.9**	41.8 ± 2.0**
Fat mass (g)	6.4 ± 0.6	7.8 ± 0.6[ns]	13.2 ± 1.5***	12.1 ± 1.3***
Lean mass (g)	22.2 ± 0.3	22.7 ± 0.4[ns]	23.1 ± 0.6[ns]	23.2 ± 0.8[ns]
Cholesterol (mg/dl)	113.5 ± 7.5	102.9 ± 14.4[ns]	135.2 ± 10.6[ns]	166.5 ± 14.2**
Triglycerides (mg/dl)	46.9 ± 6.8	48.7 ± 4.1[ns]	49.0 ± 5.9[ns]	42.1 ± 2.4[ns]
NEFA (mE/l)	0.6 ± 0.1	0.8 ± 0.1[ns]	0.7 ± 0.1[ns]	0.7 ± 0.1[ns]
Glycerol (mg/dl)	24.2 ± 1.7	33.2 ± 3.8[ns]	30.5 ± 2.5[ns]	32.9 ± 1.2[ns]
Leptin (ng/ml)	15.2 ± 2.9	15.9 ± 3.1[ns]	42.6 ± 5.5**	42.2 ± 4.9**

$n = 6$–7 mice per genotype. Values represent mean ± SEM. Statistics were performed using one-way ANOVA followed by Tukey's *post-hoc* analysis. Ns, no significance,
*$P < 0.05$,
** $P \leq 0.01$,
*** $P \leq 0.001$ compared with B6.+/Y Male (WT).

Mecp2^{flox}/Y;A*lb*-Cre display no significant increase in circulating fatty acids or glycerol (Table 1). As such, *Mecp2* loss from the liver dissociates fatty liver and insulin sensitivity.

Discussion

Thought to be entirely a neurological disorder, RTT research has focused on the role of *Mecp2* in the CNS; however, the wide variety of phenotypes in *Mecp2* null mice and RTT patients points to vital roles for *Mecp2* outside the nervous system (32–36). Here we show that *Mecp2* null male mice develop severe dyslipidemia due to aberrant transcription of rate-limiting *de novo* lipogenesis and cholesterol synthesizing enzymes in the liver. Strikingly, expression of neither *Srebp1c* nor nSREBP2, the transcriptional regulators of fatty acid and cholesterol synthesis, respectively, changed in *Mecp2*/Y liver (27,37). As such, we hypothesized that increased transcription of cholesterol and *de novo* lipogenesis enzymes results from a direct loss of MeCP2 transcriptional repression at targeted loci, rather than increased SREBP activity, similar to a liver-specific deletion of *Hdac3*.

MeCP2 represses gene transcription through association with chromatin-remodeling complexes containing Type I histone deacetylases (38,39), which cannot readily bind promoter regions in the absence of MeCP2, resulting in aberrant transcription of targets (40). In neurons, NCoR1-HDAC3 associates with MeCP2 to regulate gene transcription in an activity-dependent manner (9,10). The NCoR1-HDAC3 complex regulates a wide range of vital cellular processes: its disruption is implicated in metabolism, inflammatory pathways, and perturbed CNS development (reviewed in 41). Whole-body deletion of *Hdac3* results in embryonic death, limiting its mechanistic study to individual tissues and organ systems (42). Hepatic HDAC3 regulates the diurnal balance between gluconeogenesis and lipid synthesis thereby balancing energy oxidation versus storage during the fasted and fed states, respectively. Liver-specific deletion of *Hdac3* increases activating acetylation marks at the promoters of enzymes in the cholesterol and triglyceride synthesizing pathways, including *Sqle*. This results in aberrant transcription of the *de novo* lipogenesis pathway in a *Srebp*-independent manner, subsequently leading to fatty liver disease and increased serum cholesterol (15–17). We hypothesized that MeCP2 interacts with the NCoR-HDAC3-TBLR1 complex in the liver to repress enzyme transcription (20). Indeed, hepatic MeCP2 interacts *in vivo* with endogenous HDAC3, NCoR1, and TBLR1 in the liver. Loss of MeCP2 decreases HDAC3 binding,

resulting in an open chromatin state, as defined by increased H3K27ac marks at the *Sqle, Fasn*, and *Cd36* loci (Fig. 6). This histone modification profile in the liver is highly consistent with loss of enzymatically active HDAC3 (30).

In addition to fatty liver, *Mecp2* null mice develop glucose intolerance and hyperinsulinemia as early as four weeks of age, before onset of neurological phenotypes. Insulin resistance in these animals is global, as evidenced by poor glucose uptake in muscle and WAT when under a euglycemic, insulin clamped state. Lipolysis is significantly increased in *Mecp2* null mice at eight-weeks of age, but not as early as four-weeks. This timing suggests that increased lipolysis and subsequent WAT inflammation is a downstream effect of hyperinsulinemia and glucose intolerance. Consistent with increased lipolysis, a decreased RER in *Mecp2*/Y mice during both day and night cycles indicates a preferential shift in energy utilization from carbohydrate to lipids. This may be due to the inability of skeletal muscle to utilize glucose properly in its insulin resistant state, in which case the tissue will switch to fatty acid oxidation for energy.

Neither transport nor usage of glucose in the CNS is effected by insulin action (43,44). Glucose is transported into the brain through a gradient sink, such that a faster rate of glucose metabolism (glycolysis) in the brain allows for faster uptake of glucose from the blood via brain-specific GLUTs. As such, we hypothesize that increased glucose uptake by the *Mecp2*/Y null brain may be due to an upregulation in insulin-insensitive GLUT or abnormal neuronal glycolysis in response to synaptic hyper-excitability reported in *Mecp2* mutant neurons (45–48). Further investigation of this phenotype will shed light on this mechanism and may inform on a root cause of poor neuronal communication in the *Mecp2* mutant brain.

Here we show, for the first time, that MeCP2 directly controls expression of rate-limiting metabolic enzymes, such as *Sqle*, in the liver. As such, loss of MeCP2 from the liver causes aberrant expression of lipogenesis pathways leading to dyslipidemia and non-alcoholic fatty liver disease. Although the brain regulates energy metabolism through neuroendocrine feedback, we reasoned that MeCP2 deletion specifically from the liver would also result in fatty liver disease. Surprisingly, this is only the second time a conditional deletion of *Mecp2* outside of the CNS has been published (49). Consistent with our hypothesis, liver-specific deletion of *Mecp2* recapitulates most of the phenotypes of a whole-body deletion: the mice have increased *de novo* lipogenesis, fatty liver and increased serum cholesterol. This genetic experiment further supports a hepatocyte-autonomous
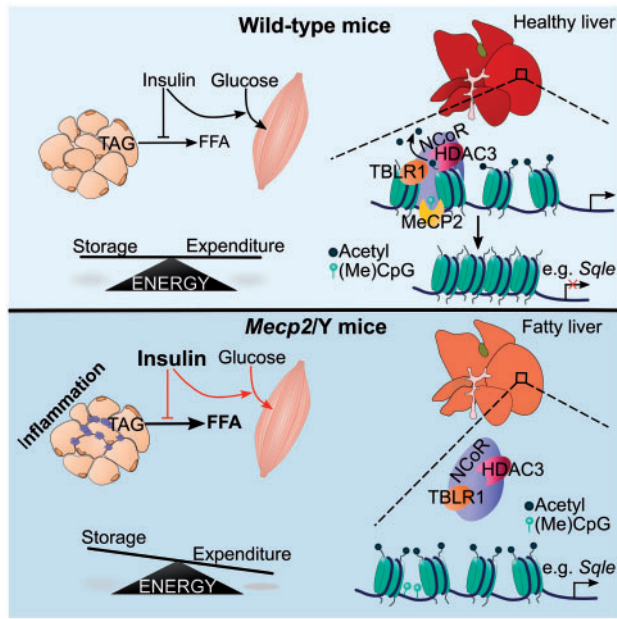
Figure 6. A schematic model of metabolic phenotypes in *Mecp2* null mice. MeCP2 co-ordinates hepatic lipid metabolism *in vivo* through binding HDAC3, which deactylates histone tails leading to reduced transcription at lipogenic loci. In the absence of MeCP2, HDAC3 fails to bind promoter regions, which prevents the removal of histone aceylation marks. This leads to downstream aberrant transcription of enzymes such as *Sqle*, which subsequently increases hepatic triglyceride and cholesterol production. *Mecp2* null mice then develop severe metabolic syndrome, including reduced insulin signaling and glucose uptake (indicated by red lines), resulting in increased lipolysis, and shifting the balance between energy storage and expenditure.

role for *Mecp2* in repression of enzymes of the cholesterol and triglyceride biosynthesis pathways. Dissociation of fatty liver and insulin resistance is reminiscent of an *Alb*-Cre induced liver deletion of *Hdac3* (17). *Mecp2* deleted from *Sim-1* or *Pomc* hypothalamic cells results in obesity, reduced *Pomc* expression, and subsequent leptin resistance (50,51). It is unknown if these hypothalamic-specific *Mecp2* deletion models develop insulin resistance. However, we would predict that dysfunctional systemic feedback between the hypothalamus, adipose, and liver in the whole-body *Mecp2* null animals account for insulin resistance and excessive lipolysis, which are absent in a liver-specific deletion of *Mecp2*.

Importantly, we found that *Mecp2* heterozygous (*Mecp2*/+) female mice develop similar metabolic phenotypes to the male null mice, indicating that a mosaic dose of MeC2 is not sufficient to maintain metabolic homeostasis in mice. Fatty liver disease has not been reported in RTT patients in the literature. However, we and others have reported abnormal cholesterol and triglycerides levels in RTT patients (21,22,52). Furthermore, glucose intolerance has been reported in pediatric RTT patients (53). Certainly, our data open the possibility that RTT should be reclassified as a neurological disorder with systemic metabolic components, and suggest that RTT patients should be examined further for metabolic anomalies. Before labelled as a monogenic neurological disorder, RTT was popularly thought to be a metabolic disease of mitochondria. Abnormal carbohydrate metabolism, increased reactive oxygen species load and poor mitochondrial function have all been reported in RTT patients or *Mecp2* mouse models (54–57). These and other metabolic anomalies can be utilized as biomarkers to alert physicians of impending complications associated with Rett syndrome.

In addition to a severe systemic dyslipidemia, we have previously reported perturbed cholesterol homeostasis in the brains of *Mecp2*/Y null mice (20). Cholesterol is a vital molecule for brain development and health as it is heavily incorporated in myelin sheaths and lipid rafts and is required for axonal guidance, synaptogenesis, and dendrite formation (58). Genetic perturbations in brain cholesterol homeostasis cause a host of severe, life-threatening neurological disorders (reviewed in 59). We showed that cholesterol-lowering statins successfully improved motor phenotypes, overall health and increased lifespan in *Mecp2* mutant mice (20). Our data here suggest that statin treatment primarily influenced improvement of phenotypes through altered brain lipids. Strikingly, statins account for only one family of numerous metabolic modulators, many of which are being developed to treat lipid accumulation in Type II diabetes, and many of which cross the blood brain barrier. Further study will illuminate new therapeutic options in highly targetable metabolic pathways that may prevent the progressing morbidities of Rett syndrome.

Materials and Methods

Animals

All animal experiments were conducted under protocols approved by local Animal Care and Use Committees in the AALAC or CCAC-accredited animal facilities at Baylor College of Medicine or the Toronto Center for Phenogenomics, respectively. Congenic 129.*Mecp2*$^{tm1.1Bird}$/Y (*Mecp2*/Y null) feature a deletion of the last two exons (exons 3–4) of the *Mecp2* transcript. *Mecp2*/Y and wild-type male offspring were obtained by backcrossing *Mecp2*$^{tm1.1Bird}$/+ females to males of the 129SvEvS6/Tac strain. *Mecp2*/Y liver-specific deletion lines (*Mecp2*^{flox}/Y; Alb-Cre), conditional-ready control (*Mecp2*^{flox}/Y) lines (exons 3 and 4 flanked by loxP sites), and wild-type littermates were obtained by crossing B6J.*Mecp2*^{tm1Bird}/+ (*Mecp2*^{flox}/+) heterozygous female mice to male mice heterozygous for the Albumin-Cre transgene on a C57BL/6J background. Mice were fed a standard diet (Harlan Teklad 2918), *ad libitum*, consisting of 18% protein, 6% fat, and 44% carbohydrates. Mice were housed in a 12-h light/dark cycle facility and were euthanized between the hours of 3 P.M. and 5 P.M. (ZT 8–10) to control for circadian rhythm fluctuations. Lean mass and fat mass was determined in live mice using a Bruker Minispec NMR body composition analyzer.

Histology

A small section of liver (~5 mm³) was extracted from *Mecp2*/Y (eight-weeks of age) and age-matched wild-type littermates. Liver was placed immediately in 10% neutral buffered formalin and was fixed for 48 h at room temperature. The liver was washed with exchanges of PBS and was incubated in increasing sucrose gradients (15% then 30%) in PBS overnight at 4°C. Tissue was frozen in OCT and 7 μm slices were prepared. Sections were then stained in 0.3% Oil Red O in isopropanol and then counterstained with hematoxylin for 5 s.

Quantitative PCR

Tissue (liver, WAT) was snap-frozen and stored at −80 until processed for RNA extraction. Details are described in Supplementary Materials. Primers are listed in Supplementary Material, Table S1.

Hyperinsulinemic-euglycemic clamps

Mice were anesthetized and a midline neck incision was made to expose the jugular vein. A microcannula was inserted into the jugular vein, threaded into the right atrium, and anchored at the venotomy site. Mice were allowed to recover for 4 days with *ad libitum* access to water and food. Following an overnight fast, the conscious mice received a primary infusion (10 uCi) and then a constant rate intravenous infusion (0.1 uCi/min) of chromatography-purified [3-^{3}H]-glucose using a syringe infusion pump. For determination of basal glucose production, blood samples were collected from the tail vein after 50, 55, and 60 min of labeled glucose infusion. After 60 min, mice received a priming bolus of insulin (40 mU/kg body weight) followed by a 2-h insulin infusion (4 mU/kg/min). Simultaneously, 10% glucose was infused using another infusion pump at a rate adjusted to maintain the blood glucose level at 100–140 mg/dl (euglycemia). Blood glucose concentration was measured every 10 min by a glucometer. At 100, 110, and 120 min, blood was collected to measure HGP under clamped conditions. To estimate insulin-stimulated GLUT activity in individual tissues 2-[^{14}C]deoxyglucose was administered as a bolus (10 uCi) at 45 min before the end of the clamps. After 120 min, mice were euthanized and tissues were extracted. Brain regions were rapidly dissected from both hemispheres of the brain. Thalamic and hypothalamic tissue was pooled. Glucose uptake in different tissues was calculated from plasma by tissue enrichment of 2-[^{14}C]deoxyglucose by gas chromatography-mass spectrometry.

Tolerance tests and lipolysis analysis

In vivo lipolysis analyses were performed by the Diabetes and Endocrinology Research Center at BCM. Details are described in Supplementary Materials.

Nuclear extraction

Freshly dissected liver (50 mg) was washed with 1X volume of ice-cold PBS and centrifuged at 500 g for 5 min at 4°C. Tissue was then transferred cleanly to a dounce homogenizer on ice containing 500 μl of cold NP40 lysis buffer (10 mM Hepes pH7.9, 3 mM MgCl$_2$, 10 mM KCl, 0.5% NP40, 0.5mM DTT, and Complete EDTA-free protease inhibitor cocktail (Roche, CA, USA)). Tissue was incubated in buffer on ice for 45 min and then tissue was disrupted with 10 strokes of the tight pestle in the dounce tissue homogenizer. Homogenized tissue was transferred into a new, cold microfuge tube and centrifuged at 2000 g for 10 min at 4°C. The supernatant was removed and the pellet was resuspended in 250 μl of Benzonase extraction buffer (10 mM Hepes pH7.9, 3 mM MgCl$_2$, 280 mM NaCl, 0.2 mM EDTA pH8.0, 0.5% NP40, 0.5 mM DTT, and Complete EDTA-free protease inhibitor cocktail) with 250 U of Benzonase. Nuclei were incubated in extraction buffer for 1 h on at rotator at 4°C. Following incubation, lysates were centrifuged at 17 000g for 20 min at 4°C. Lysates were snap frozen and stored at −80.

Co-immunoprecipitation

IP was carried out using the Millipore Catch and Release kit (Millipore, MA, USA). Following the instructions, 500 μg of nuclear lysates was incubated with 12 μg of anti-HDAC3 (ab7030), 10 μg of anti-HDAC3 (Upstate, 06-890), or 10 μg of anti-HDAC3 (SantaCruz, H-303) at 4°C for 3 h. Following elution, half of the immunoprecipitated sample was loaded onto an SDS-PAGE gel

for downstream western blotting. Input samples represent 25 μg of total nuclear extracted protein.

Western blotting

The following antibodies were used for western blotting: anti-MeCP2 (Millipore 07-013) at a concentration of 1:700 in 3% Milk-PBS; anti-SREBP2 (ab30682) at a concentration of 1:400 in 5% Milk-TBST; anti-GAPDH (Cell Signaling 5174) at a concentration of 1:8000 in 5% Milk-TBST; anti-NCoR1 (sc-1609) at a concentration of 1:450 in 1% casein-TBST; anti-TBLR1 at a concentration of 1:1200 in 1% casein-TBST. For co-IP, a light-chain specific secondary antibody (Jackson ImmunoResearch) was used to avoid heavy chain detection at 50kDa. Quantification of band intensity was achieved using ImageJ (NIH) and normalized to GAPDH.

Chromatin-IP

ChIP was performed as described in (60). Details are provided in Supplementary Materials.

Indirect calorimetry

Respiratory metabolic function was assessed using the Oxymax Deluxe System indirect calorimeter equal flow eight chamber system (Columbus Instruments, Columbus, Ohio) and analyzed using Oxymax Windows V3.32 Software. Details are described in the Supplementary Materials.

Subjective health assessments

Mice were assayed for general health once per week from 5 weeks of age to 24-weeks of age. Scoring was blinded by genotype. Mice were scored using the assessment published in (61), where a score of 0 is not different from wildtype, 1 is more severe, and 2 is very severe. Mice were assessed for limbclasping, tremors, home-cage activity, and grooming for a combined possible score of 0–8.

Rotarod

At 5-months of age, male mice were placed on a grooved rotating rod at a speed of 4 r.p.m. Over the course of 5 min, the revolution rate increased steadily to a maximum of 40 r.p.m. The time each mouse stayed on the rod was recorded for four trials spread across two consecutive days, totaling eight trials for each mouse, with a 30-min break between trials. A trial ended when the mouse fell from the rotating rod, spun with the rod for two consecutive revolutions, or successfully stayed on the rod for 5 min.

Statistics

Values are expressed at mean ± SEM. The significance of the differences in mean values among different groups was evaluated by two-tailed Student *t*-tests or, for comparing means of more than two groups, one-way ANOVA followed by Tukey's *post-hoc* analysis. P-values < 0.05 were considered statistically significant (P< 0.05 =*, P ≤ 0.01 = **, P ≤ 0.001 =***). Linear regression, Student *t*-test, and ANOVA was analyzed using GraphPad Prism 6.

Supplementary Material

Acknowledgements

Funding

References

1. Amir, R.E., Van den Veyver, I.B., Wan, M., Tran, C.Q., Francke, U. and Zoghbi, H.Y. (1999) Rett syndrome is caused by mutations in X-linked MECP2, encoding methyl-CpG-binding protein 2. *Nat. Genet.*, **23**, 185–188.

2. Braunschweig, D., Simcox, T., Samaco, R.C. and LaSalle, J.M. (2004) X-Chromosome inactivation ratios affect wild-type MeCP2 expression within mosaic Rett syndrome and Mecp2−/+ mouse brain. *Hum. Mol. Genet.*, **13**, 1275–1286.

3. Guy, J., Hendrich, B., Holmes, M., Martin, J.E. and Bird, A. (2001) A mouse Mecp2-null mutation causes neurological symptoms that mimic Rett syndrome. *Nat. Genet.*, **27**, 322–326.

4. Katz, D.M., Berger-Sweeney, J.E., Eubanks, J.H., Justice, M.J., Neul, J.L., Pozzo-Miller, L., Blue, M.E., Christian, D., Crawley, J.N., Giustetto, M. *et al.* (2012) Preclinical research in Rett syndrome: setting the foundation for translational success. *Dis. Model. Mech.*, **5**, 733–745.

5. Young, J.I. and Zoghbi, H.Y. (2004) X-Chromosome Inactivation Patterns Are Unbalanced and Affect the Phenotypic Outcome in a Mouse Model of Rett Syndrome. *Am. J. Hum. Genet.*, **74**, 511–520.

6. Adams, V.H., McBryant, S.J., Wade, P.A., Woodcock, C.L. and Hansen, J.C. (2007) Intrinsic Disorder and Autonomous Domain Function in the Multifunctional Nuclear Protein, MeCP2. *J. Biol. Chem.*, **282**, 15057–15064.

7. Skene, P.J., Illingworth, R.S., Webb, S., Kerr, A.R.W., James, K.D., Turner, D.J., Andrews, R. and Bird, A.P. (2010) Neuronal MeCP2 is expressed at near histone-octamer levels and globally alters the chromatin state. *Mol. Cell*, **37**, 457–468.

8. Ausió, J., Paz, AM. de and Esteller, M. (2014) MeCP2: the long trip from a chromatin protein to neurological disorders. *Trends Mol. Med.*, **20**, 487–498.

9. Ebert, D.H., Gabel, H.W., Robinson, N.D., Kastan, N.R., Hu, L.S., Cohen, S., Navarro, A.J., Lyst, M.J., Ekiert, R., Bird, A.P. *et al.* (2013) Activity-dependent phosphorylation of MeCP2 threonine 308 regulates interaction with NCoR. *Nature*, **499**, 341–345.

10. Lyst, M.J., Ekiert, R., Ebert, D.H., Merusi, C., Nowak, J., Selfridge, J., Guy, J., Kastan, N.R., Robinson, N.D., de Lima Alves, F. *et al.* (2013) Rett syndrome mutations abolish the interaction of MeCP2 with the NCoR/SMRT co-repressor. *Nat. Neurosci.*, **16**, 898–902.

11. Guenther, M.G., Barak, O. and Lazar, M.A. (2001) The SMRT and N-CoR Corepressors Are Activating Cofactors for Histone Deacetylase 3. *Mol. Cell. Biol.*, **21**, 6091–6101.

12. Li, J., Wang, J., Wang, J., Nawaz, Z., Liu, J.M., Qin, J. and Wong, J. (2000) Both corepressor proteins SMRT and N-CoR exist in large protein complexes containing HDAC3. *Embo J.*, **19**, 4342–4350.

13. Heckman, L.D., Chahrour, M.H. and Zoghbi, H.Y. (2014) Rett-causing mutations reveal two domains critical for MeCP2 function and for toxicity in MECP2 duplication syndrome mice. *eLife*, **3**

14. Alenghat, T., Meyers, K., Mullican, S.E., Leitner, K., Adeniji-Adele, A., Avila, J., Bućan, M., Ahima, R.S., Kaestner, K.H. and Lazar, M.A. (2008) Nuclear receptor corepressor and histone deacetylase 3 govern circadian metabolic physiology. *Nature*, **456**, 997–1000.

15. Feng, D., Liu, T., Sun, Z., Bugge, A., Mullican, S.E., Alenghat, T., Liu, X.S. and Lazar, M.A. (2011) A Circadian Rhythm Orchestrated by Histone Deacetylase 3 Controls Hepatic Lipid Metabolism. *Science*, **331**, 1315–1319.

16. Knutson, S.K., Chyla, B.J., Amann, J.M., Bhaskara, S., Huppert, S.S. and Hiebert, S.W. (2008) Liver-specific deletion of histone deacetylase 3 disrupts metabolic transcriptional networks. *Embo J*, **27**, 1017–1028.

17. Sun, Z., Miller, R.A., Patel, R.T., Chen, J., Dhir, R., Wang, H., Zhang, D., Graham, M.J., Unterman, T.G., Shulman, G.I. *et al.* (2012) Hepatic Hdac3 promotes gluconeogenesis by repressing lipid synthesis and sequestration. *Nat. Med.*, **18**, 934–942.

18. Gill, S., Stevenson, J., Kristiana, I. and Brown, A.J. (2011) Cholesterol-dependent degradation of squalene monooxygenase, a control point in cholesterol synthesis beyond HMG-CoA reductase. *Cell Metab.*, **13**, 260–273.

19. Hidaka, Y., Satoh, T. and Kamei, T. (1990) Regulation of squalene epoxidase in HepG2 cells. *J. Lipid Res.*, **31**, 2087–2094.

20. Buchovecky, C.M., Turley, S.D., Brown, H.M., Kyle, S.M., McDonald, J.G., Liu, B., Pieper, A.A., Huang, W., Katz, D.M., Russell, D.W. *et al.* (2013) A suppressor screen in Mecp2 mutant mice implicates cholesterol metabolism in Rett syndrome. *Nat. Genet.*, **45**, 1013–1020.

21. Justice, M.J., Buchovecky, C.M., Kyle, S.M. and Djukic, A. (2013) A role for metabolism in Rett syndrome pathogenesis: New clinical findings and potential treatment targets. *Rare Dis. Austin Tex.*, **1**, e27265.

22. Segatto, M., Trapani, L., Di Tunno, I., Sticozzi, C., Valacchi, G., Hayek, J. and Pallottini, V. (2014) Cholesterol metabolism is altered in rett syndrome: a study on plasma and primary cultured fibroblasts derived from patients. *PLoS One*, **9**, e104834.

23. Guillot, F., Misslin, P. and Lemaire, M. (1993) Comparison of fluvastatin and lovastatin blood-brain barrier transfer using in vitro and in vivo methods. *J. Cardiovasc. Pharmacol.*, **21**, 339–346.

24. Saheki, A., Terasaki, T., Tamai, I. and Tsuji, A. (1994) In vivo and in vitro blood-brain barrier transport of 3-hydroxy-3-methylglutaryl coenzyme A (HMG-CoA) reductase inhibitors. *Pharm. Res.*, **11**, 305–311.

25. Matsumoto, M., Ogawa, W., Akimoto, K., Inoue, H., Miyake, K., Furukawa, K., Hayashi, Y., Iguchi, H., Matsuki, Y., Hiramatsu, R. *et al.* (2003) PKClambda in liver mediates insulin-induced SREBP-1c expression and determines both hepatic lipid content and overall insulin sensitivity. *J. Clin. Invest*, **112**, 935–944.

26. Shimomura, I., Matsuda, M., Hammer, R.E., Bashmakov, Y., Brown, M.S. and Goldstein, J.L. (2000) Decreased IRS-2 and increased SREBP-1c lead to mixed insulin resistance and

sensitivity in livers of lipodystrophic and ob/ob mice. *Mol. Cell*, **6**, 77–86.

27. Horton, J.D., Goldstein, J.L. and Brown, M.S. (2002) SREBPs: activators of the complete program of cholesterol and fatty acid synthesis in the liver. *J. Clin. Invest.*, **109**, 1125–1131.

28. Guilherme, A., Virbasius, J.V., Puri, V. and Czech, M.P. (2008) Adipocyte dysfunctions linking obesity to insulin resistance and type 2 diabetes. *Nat. Rev. Mol. Cell Biol.*, **9**, 367–377.

29. Tschöp, M.H., Speakman, J.R., Arch, J.R.S., Auwerx, J., Brüning, J.C., Chan, L., Eckel, R.H., Farese, R.V., Galgani, J.E., Hambly, C. *et al.* (2012) A guide to analysis of mouse energy metabolism. *Nat. Methods*, **9**, 57–63.

30. You, S.H., Lim, H.W., Sun, Z., Broache, M., Won, K.J. and Lazar, M.A. (2013) Nuclear receptor co-repressors are required for the histone-deacetylase activity of HDAC3 in vivo. *Nat. Struct. Mol. Biol.*, **20**, 182–187.

31. Samaco, R.C., Fryer, J.D., Ren, J., Fyffe, S., Chao, H.T., Sun, Y., Greer, J.J., Zoghbi, H.Y. and Neul, J.L. (2008) A partial loss of function allele of Methyl-CpG-binding protein 2 predicts a human neurodevelopmental syndrome. *Hum. Mol. Genet.*, **17**, 1718–1727.

32. Chahrour, M. and Zoghbi, H.Y. (2007) The story of Rett syndrome: from clinic to neurobiology. *Neuron*, **56**, 422–437.

33. Gong, M., Liu, J., Sakurai, R., Corre, A., Anthony, S. and Rehan, V.K. (2015) Perinatal nicotine exposure suppresses PPARγ epigenetically in lung alveolar interstitial fibroblasts. *Mol. Genet. Metab.*, **114**, 604–612.

34. Hara, M., Takahashi, T., Mitsumasu, C., Igata, S., Takano, M., Minami, T., Yasukawa, H., Okayama, S., Nakamura, K., Okabe, Y. *et al.* (2015) Disturbance of cardiac gene expression and cardiomyocyte structure predisposes Mecp2-null mice to arrhythmias. *Sci. Rep*, **5**.

35. Hu, B., Gharaee-Kermani, M., Wu, Z. and Phan, S.H. (2011) Essential role of MeCP2 in the regulation of myofibroblast differentiation during pulmonary fibrosis. *Am. J. Pathol.*, **178**, 1500–1508.

36. Li, C., Jiang, S., Liu, S.Q., Lykken, E., Zhao, L., Sevilla, J., Zhu, B. and Li, Q.J. (2014) MeCP2 enforces Foxp3 expression to promote regulatory T cells' resilience to inflammation. *Proc. Natl. Acad. Sci. USA*, **111**, E2807–E2816.

37. Murphy, C., Ledmyr, H., Ehrenborg, E. and Gåfvels, M. (2006) Promoter analysis of the murine squalene epoxidase gene. Identification of a 205 bp homing region regulated by both SREBP'S and NF-Y. *Biochim. Biophys. Acta*, **1761**, 1213–1227.

38. Bienvenu, T. and Chelly, J. (2006) Molecular genetics of Rett syndrome: when DNA methylation goes unrecognized. *Nat. Rev. Genet.*, **7**, 415–426.

39. Stancheva, I., Collins, A.L., Van den Veyver, I.B., Zoghbi, H. and Meehan, R.R. (2003) A mutant form of MeCP2 protein associated with human Rett syndrome cannot be displaced from methylated DNA by notch in Xenopus embryos. *Mol. Cell*, **12**, 425–435.

40. Martinowich, K., Hattori, D., Wu, H., Fouse, S., He, F., Hu, Y., Fan, G. and Sun, Y.E. (2003) DNA Methylation-Related Chromatin Remodeling in Activity-Dependent Bdnf Gene Regulation. *Science*, **302**, 890–893.

41. Karagianni, P. and Wong, J. (2007) HDAC3: taking the SMRT-N-CoRrect road to repression. *Oncogene*, **26**, 5439–5449.

42. Bhaskara, S., Chyla, B.J., Amann, J.M., Knutson, S.K., Cortez, D., Sun, Z.W. and Hiebert, S.W. (2008) Deletion of Histone Deacetylase 3 Reveals Critical Roles in S Phase Progression and DNA Damage Control. *Mol. Cell*, **30**, 61–72.

43. Mergenthaler, P., Lindauer, U., Dienel, G.A. and Meisel, A. (2013) Sugar for the brain: the role of glucose in physiological and pathological brain function. *Trends Neurosci.*, **36**, 587–597.

44. Banks, W.A., Owen, J.B. and Erickson, M.A. (2012) Insulin in the brain: there and back again. *Pharmacol. Ther*, **136**, 82–93.

45. Calfa, G., Hablitz, J.J. and Pozzo-Miller, L. (2011) Network hyperexcitability in hippocampal slices from Mecp2 mutant mice revealed by voltage-sensitive dye imaging. *J. Neurophysiol.*, **105**, 1768–1784.

46. Zhang, W., Peterson, M., Beyer, B., Frankel, W.N. and Zhang, Z. (2014) Loss of MeCP2 from forebrain excitatory neurons leads to cortical hyperexcitation and seizures. *J. Neurosci. Off. J. Soc. Neurosci.*, **34**, 2754–2763.

47. Kron, M., Howell, C.J., Adams, I.T., Ransbottom, M., Christian, D., Ogier, M. and Katz, D.M. (2012) Brain Activity Mapping in Mecp2 Mutant Mice Reveals Functional Deficits in Forebrain Circuits, Including Key Nodes in the Default Mode Network, that are Reversed with Ketamine Treatment. *J. Neurosci. Off. J. Soc. Neurosci*, **32**, 13860–13872.

48. Lundgaard, I., Li, B., Xie, L., Kang, H., Sanggaard, S., Haswell, J.D.R., Sun, W., Goldman, S., Blekot, S., Nielsen, M. *et al.* (2015) Direct neuronal glucose uptake heralds activity-dependent increases in cerebral metabolism. *Nat. Commun.*, **6**, 6807.

49. Conti, V., Gandaglia, A., Galli, F., Tirone, M., Bellini, E., Campana, L., Kilstrup-Nielsen, C., Rovere-Querini, P., Brunelli, S. and Landsberger, N. (2015) MeCP2 affects skeletal muscle growth and morphology through non cell-autonomous mechanisms. *PLoS One*, **10**.

50. Fyffe, S.L., Neul, J.L., Samaco, R.C., Chao, H.T., Ben-Shachar, S., Moretti, P., McGill, B.E., Goulding, E.H., Sullivan, E., Tecott, L.H. *et al.* (2008) Deletion of Mecp2 in Sim1-expressing neurons reveals a critical role for MeCP2 in feeding behavior, aggression, and the response to stress. *Neuron*, **59**, 947–958.

51. Wang, X., Lacza, Z., Sun, Y.E. and Han, W. (2014) Leptin resistance and obesity in mice with deletion of methyl-CpG-binding protein 2 (MeCP2) in hypothalamic pro-opiomelanocortin (POMC) neurons. *Diabetologia*, **57**, 236–245.

52. Sticozzi, C., Belmonte, G., Pecorelli, A., Cervellati, F., Leoncini, S., Signorini, C., Ciccoli, L., De Felice C., Hayek J. and Valacchi, G., (2013) Scavenger receptor B1 post-translational modifications in Rett syndrome. *FEBS Lett.*, 10.1016/j.febslet.2013.05.042.

53. Cooke, D.W., Naidu, S., Plotnick, L. and Berkovitz, G.D. (1995) Abnormalities of thyroid function and glucose control in subjects with Rett syndrome. *Horm. Res.*, **43**, 273–278.

54. Cronk, J.C., Derecki, N.C., Ji, E., Xu, Y., Lampano, A.E., Smirnov, I., Baker, W., Norris, G.T., Marin, I., Coddington, N. *et al.* (2015) Methyl-CpG binding protein 2 regulates microglia and macrophage gene expression in response to inflammatory stimuli. *Immunity*, **42**, 679–691.

55. De Felice, C., Della Ragione, F., Signorini, C., Leoncini, S., Pecorelli, A., Ciccoli, L., Scalabrì, F., Marracino, F., Madonna, M., Belmonte, G. *et al.* (2014) Oxidative brain damage in Mecp2-mutant murine models of Rett syndrome. *Neurobiol. Dis.*, **68**, 66–77.

56. Matsuishi, T., Urabe, F., Percy, A.K., Komori, H., Yamashita, Y., Schultz, R.S., Ohtani, Y., Kuriya, N. and Kato, H. (1994) Abnormal carbohydrate metabolism in cerebrospinal fluid in rett syndrome. *J. Child Neurol.*, **9**, 26–30.

57. Müller, M. and Can, K. (2014) Aberrant redox homoeostasis and mitochondrial dysfunction in Rett syndrome. *Biochem. Soc. Trans.*, **42**, 959–964.

58. Pfrieger, F.W. and Ungerer, N. (2011) Cholesterol metabolism in neurons and astrocytes. *Prog. Lipid Res.*, **50**, 357–371.

59. Kanungo, S., Soares, N., He, M. and Steiner, R.D. (2013) Sterol metabolism disorders and neurodevelopment—an update. *Dev. Disabil. Res. Rev.*, **17**, 197–210.

60. Schmidt, D., Wilson, M.D., Spyrou, C., Brown, G.D., Hadfield, J. and Odom, D.T. (2009) ChIP-seq: using high-throughput sequencing to discover protein-DNA interactions. *Methods San Diego Calif*, **48**, 240–248.

61. Guy, J., Gan, J., Selfridge, J., Cobb, S. and Bird, A. (2007) Reversal of neurological defects in a mouse model of Rett syndrome. *Science*, **315**, 1143–1147.